

# Structural Determinants of Herpesvirus Entry Mediator Recognition by Murine B and T Lymphocyte Attenuator<sup>1</sup>

Christopher A. Nelson,\* Marcel D. Fremont,\* John R. Sedy,‡ Paula S. Norris,‡ Carl F. Ware,‡ Kenneth M. Murphy,\* and Daved H. Fremont<sup>2\*†</sup>

The B and T lymphocyte attenuator (BTLA) appears to act as a negative regulator of T cell activation and growth. BTLA specifically interacts with herpesvirus entry mediator (HVEM), a member of the TNFR family. Herein, we have undertaken surface plasmon resonance studies to quantitatively assess BTLA and HVEM ectodomain interactions. We find that soluble BALB/cJ BTLA engages HVEM with an equilibrium affinity of  $0.97 \pm 0.19 \mu\text{M}$  while the C57BL/6 BTLA binds slightly better with an equilibrium affinity of  $0.42 \pm 0.06 \mu\text{M}$ . Despite its lower affinity for HVEM, the kinetic half-life of BALB/cJ BTLA complexes are twice as long as observed for C57BL/6 BTLA (4 vs 2 s). To further explore these interactions, we solved the crystal structure of a murine BTLA (BALB/cJ) ectodomain at 1.8-Å resolution, revealing a  $\beta$  sandwich fold with strong similarity to I-set members of the Ig superfamily. Using a structure-based mutagenesis strategy, we then examined the individual contributions of 26 BTLA surface-exposed residues toward HVEM binding. Four single-site substitutions were identified that decrease HVEM binding below detectable levels and two that decrease binding by more than half. All six of these cluster at the edge of the  $\beta$  sandwich in a membrane distal patch formed primarily from the A and G strands. This patch falls within the contacting surface recently revealed in the crystal structure of the human BTLA-HVEM cocomplex. The critical binding residues identified here are highly conserved across species, suggesting that BTLA employs a conserved binding mode for HVEM recognition. *The Journal of Immunology*, 2008, 180: 940–947.

The B and T lymphocyte attenuator is a type I transmembrane glycoprotein expressed at high levels on activated T cells and resting B cells and at lower levels on naive T cells, NK cells, bone marrow-derived dendritic cells, and splenic macrophages (1, 2). The primary endogenous binding partner for B and T lymphocyte attenuator (BTLA)<sup>3</sup> is herpesvirus entry mediator (HVEM), also called TNFRSF-14 (3, 4), a member of the TNFR family. HVEM is known for its ability to provide costimulatory signals to T cells in response to the TNF-related cytokine LIGHT (5, 6). Clustering of HVEM by LIGHT initiates signaling through TNFR-associated factor adaptors resulting in the activation of NF- $\kappa$ B, JNK, and adapter protein 1 signaling pathways (7, 8).

Recent evidence suggests that BTLA-HVEM interactions serve to regulate T cell development and activation events (4, 9). These interactions remain unique as the only example of signaling cross-

talk between the Ig and TNFR families of surface receptors. The cytoplasmic tail of murine BTLA contains a potential growth factor receptor-bound protein 2 binding site as well as an ITIM and an immunoreceptor tyrosine-based switch motif (10). These tyrosine-based motifs undergo phosphorylation upon colligation of BTLA with the TCR (11) and are conserved in BTLA orthologs from zebra fish to humans (12), implying a conserved biological role. In vitro studies document the ability of BTLA to act as a negative regulator, although the cytosolic factors responsible remain unclear (13–15). Ab cross-linking of BTLA inhibits IL-2 production by T cell hybridomas in response to anti-CD3 stimulation (11). Likewise, coimmobilized anti-BTLA Ab or HVEM-Fc fusion protein has been shown to reduce the proliferation and cytokine production by purified T cells in response to anti-CD3 treatment (1, 3, 16–19). These results are consistent with the proposal that BTLA acts as a coinhibitory receptor, exerting its effect when clustered in proximity with the TCR. Indeed, genetic loss of BTLA leads to an increase in T cell responsiveness, providing in vivo support for an inhibitory role. Ab blockade of BTLA or HVEM promotes the rapid rejection of partially MHC class I- or class II-mismatched allografts (20). In addition, BTLA<sup>-/-</sup> mice show increased severity and duration of disease when challenged with experimentally induced autoimmune encephalomyelitis (11), and they exhibit prolonged airway inflammation when challenged with inhaled Ag (21). However, the phenotype of heightened immune responsiveness in these animals may not be a direct result of the loss of coinhibitory signal from the T cells themselves, but instead, may be due to an increase in the abundance of CD8<sup>+</sup> memory T cells which has been reported to occur in both BTLA<sup>-/-</sup> and HVEM<sup>-/-</sup> mice (9).

The extracellular portion of HVEM consists of four cysteine-rich domains (CRDs) (22) or pseudo repeats, each ~40 residues in length that are characteristic of the TNFR superfamily (22–24). HVEM binds LIGHT, a TNF-related trimeric cytokine. By

\*Department of Pathology and Immunology and <sup>†</sup>Department of Biochemistry and Molecular Biophysics, Washington University School of Medicine, St. Louis, MO 63110; and <sup>‡</sup>Division of Molecular Immunology, La Jolla Institute for Allergy and Immunology, San Diego, CA 92121

Received for publication September 4, 2007. Accepted for publication October 28, 2007.

The costs of publication of this article were defrayed in part by the payment of page charges. This article must therefore be hereby marked *advertisement* in accordance with 18 U.S.C. Section 1734 solely to indicate this fact.

<sup>1</sup> This work was supported by Midwest Center for Structural Genomics, National Institutes of Health Grant GM62414-04 (to D.H.F.).

<sup>2</sup> Address correspondence and reprint requests to Dr. Daved H. Fremont, Department of Pathology and Immunology, Washington University School of Medicine, 660 South Euclid Avenue, Campus Box 8118, St. Louis, MO 63110. E-mail address: fremont@wustl.edu

<sup>3</sup> Abbreviations used in this paper: BTLA, B and T lymphocyte attenuator; HVEM, herpesvirus entry mediator; CRD, cysteine-rich domain; PD-1, programmed death receptor 1; ESMS, electrospray mass spectrometry; SPR, surface plasmon resonance; GVHD, graft-versus-host disease.

Copyright © 2008 by The American Association of Immunologists, Inc. 0022-1767/08/\$2.00

analogy with related systems (e.g., TNFR1/TNF $\beta$  (25)) and from mutagenesis studies (26), it is predicted that LIGHT will contact HVEM primarily through an elongated surface spanning the CRD2 and CRD3 domains. BTLA binds HVEM on the opposite side of the receptor, in the CRD1 domain (4, 27), in a region that has come to be called the "DARC" site of HVEM (16) because it contains the attachment site for the envelope glycoprotein D of HSV-1 (22, 28). In turn, the binding site for HVEM on BTLA is targeted by UL144, a TNFR-like decoy encoded by human CMV (16). UL144 binds BTLA, but not LIGHT, and inhibits T cell proliferation, presumably by exploiting the inhibitory cosignaling function of BTLA.

A crystal structure revealing specific details of the interaction between human BTLA and HVEM was recently reported (29). BTLA recognizes, as its principal binding target, an extended  $\beta$ -strand located in the membrane-distal region of the HVEM CRD1 domain, specifically HVEM  $\beta$ -strand residues 35–39 (TVCEP). These residues form an intramolecular anti-parallel  $\beta$ -sheet with residues 122–128 (NLIESHS) of human BTLA. When alanine-scanning mutagenesis was used to evaluate the binding contributions of 15 individual HVEM side chains, the three most disruptive substitutions were residues involved in the formation of the  $\beta$ -strand, confirming the intramolecular  $\beta$ -sheet as a central feature of the binding interface. These results suggest BTLA uses a unique binding surface, distinct from that used by coinhibitory receptors of the related CD28 family. In this study, we demonstrate that the human BTLA-HVEM results are relevant to the mouse BTLA-HVEM system. There existed some reason for caution, since the binding specificities of the two TNFR are known to differ. Human HVEM binds the TNF-related human cytokine lymphotoxin  $\alpha$  in addition to human LIGHT. In contrast, mouse HVEM does not bind mouse lymphotoxin  $\alpha$  and binds only weakly to mouse LIGHT (30). From sequence comparisons, only 11 of 17 human BTLA amino acids that bury at least 25% of their surface accessible area upon HVEM binding are identically conserved in mouse BTLA (29). Similarly, only 12 of 20 HVEM residues that bury solvent accessible surface upon BTLA binding are identically conserved in mouse HVEM (29). No crystal structure yet exists for mouse HVEM; therefore, it is difficult to predict the exact configuration of the mouse BTLA-HVEM binding interface. However, we have obtained a crystal structure of the extracellular region of murine BTLA (BALB/cJ allele) and used that information to design a series of singly substituted BTLA proteins for affinity studies by Scatchard analysis. Of 26 single-site substitutions tested, we identified 4 that abolish HVEM binding and 2 others that lower binding by more than 2-fold. Our results confirm that murine and human BTLA engage HVEM using a conserved binding motif and represent the first functional characterization of individual BTLA residues involved in HVEM binding.

## Materials and Methods

### Cloning, expression, and protein refolding

A cDNA fragment encoding the mature N-terminal ectodomain of BTLA was inserted between the *Nco*I and *Xho*I sites of the bacterial expression vector pET-21a (EMD Biosciences) (aa 30 through 121, as numbered in accession no. AAP44002). This plasmid was introduced into BL21(DE3)-RIL codon (+) *Escherichia coli* cells (Stratagene) for expression. Recombinant protein was recovered as an insoluble inclusion body pellet, solubilized in guanidine hydrochloride, and then renatured by rapid dilution in refolding buffer consisting of 1 M arginine, 100 mM Tris-HCl, 2 mM EDTA, 200  $\mu$ M PMSF, 5 mM reduced glutathione, and 0.5 mM oxidized glutathione at a final pH of 8.3. After 24 h, the soluble refolded protein was collected in a stirred cell concentrator using YM10 membrane (Millipore), passed through a 0.45- $\mu$ m filter, and subjected to sizing on Superdex 200 (GE Health Sciences). The resulting native protein eluted from size exclusion chromatography at  $\sim$ 14 kDa, the position predicted for the BTLA

monomer. The final recombinant fragment contained no extraneous tags. Its identity was confirmed by electrospray mass spectrometry (ESMS), the observed mass being consistent with two disulfide bonds in each molecule. Fractions containing mono-disperse protein were pooled and kept at 4°C in sizing buffer (25 mM HEPES (pH 7.5) and 150 mM sodium chloride with 0.01% sodium azide). Mutagenesis of the pET-21-BTLA plasmid was performed using a QuickChange site-directed mutagenesis kit (Stratagene).

To prepare a sample for ESMS, 10  $\mu$ g of protein was diluted to 100  $\mu$ l in water and mixed with 100  $\mu$ l of 20% trichloroacetic acid. This mixture was held on ice for 30 min. The sample was spun in a microfuge at 16,000  $\times$  g at 4°C for 20 min. The precipitate was washed with 300  $\mu$ l of cold acetone and spun again at 16,000  $\times$  g at 4°C for 5 min. The protein pellet was air dried and resuspended in 20  $\mu$ l of 60% acetonitrile with 0.1% formic acid for analysis. ESMS of the protein used for the crystallization trials (BALB/cJ) yielded an observed  $M_r$  14,428 Da. The sequence (M)-EKAT...QNSS\* predicts a  $M_r$  14,126.89 Da. The observed weight indicates two disulfide bonds per monomer with the fifth cysteine capped by glutathione (14,428.00 Da = 14,126.89 fragment – 5.04 Da for 5 hydrogens plus 306.3 Da for oxidized glutathione).

### Crystallization conditions

The crystals were grown at 293°K in hanging drops by mixing an equal volume of BTLA protein at 9.6 mg/ml in 20 mM HEPES (pH 7.4) with well solution containing 10 mM cadmium chloride, 100 mM citric acid/sodium hydroxide (pH 5.8), 220 mM ammonium acetate, 26% polyethylene glycol 4000, and 10 mM trimethylamine-HCl.

### Data collection and processing

Diffraction data were collected at the Advanced Light Source (ALS) synchrotron (beamline 4.2.2) using a charge-coupled device detector (Noir-1). Because cadmium ions were required for crystal growth, we attempted to derive experimental phase from their anomalous and dispersive scattering differences. Two datasets were collected from a single crystal. A quick pass (to minimize the effects of radiation damage in the single-wavelength anomalous dispersion phasing) was collected at 2.06637 Å wavelength to a resolution of 2.25 Å and a slow pass (for model refinement) was collected at 1.54978 Å wavelength to a resolution of 1.8 Å. Although both occur on the high-energy side of the absorption edge ( $L_1 \sim 3.0857$  Å), a solution was feasible because of the relatively large  $f''$  and small  $f'$  inherent in the 2.06637 Å dataset. Data processing with *d\*Trek* (31) revealed that the crystal belonged to orthorhombic space group  $P2_12_12_1$  ( $a = 36.67$  Å,  $b = 37.54$  Å, and  $c = 90.15$  Å). The asymmetric unit of the crystal contained a single BTLA monomer. The total solvent content was  $\sim$ 44% with a Matthews coefficient of 2.20 Å<sup>3</sup>(Da).

### Model building and refinement

An analysis of the anomalous differences in the 2.06637 Å dataset, using the heavy atom search program from the crystallography and NMR system software suite (32), revealed two relatively strong cadmium peaks per molecule. The initial phases were calculated from these positions using both datasets. Phases were further improved in SHARP (33) by solvent flattening and histogram matching. The map calculated from the improved phases (40.0–2.25 Å) was sufficient to trace the backbone structure of the protein. A partial model was generated by the autobuild feature of ARP/wARP (34) spanning 95 of 122 residues in three chains with a connectivity index of 0.92. This model was inspected in the program O (35). Only minor corrections were required before refinement in the crystallography and NMR system software suite. Both 2Fo-Fc and Fo-Fc maps were used between refinement cycles for manual building and to locate solvent molecules. All reflections (40.0–1.8 Å) from the 1.54978 Å dataset were included throughout the refinement calculations, except those set aside for free R factor cross-validation (5%). The final model yielded an  $R_{\text{free}}$  of 20.6% and  $R_{\text{work}}$  of 26.9%; additional refinement statistics are summarized in Table I. The first 10, and last 7, residues of the 121 aa BTLA ectodomain are disordered in the crystal structure. Removal of the first 10 residues had no significant effect on HVEM binding. The quality of the model was checked with PROCHECK (36). Solvent accessibilities were calculated with NACCESS (probe radius, 1.4 Å) (37). Molecular diagrams were drawn using the programs GRASP (38) and Pymol (39).

### Atomic coordinates and structure factors

The atomic coordinates and structure factors (accession code 1XAU) have been deposited, in the Protein Data Bank, Research Collaboratory for Structural Bioinformatics (Rutgers University, New Brunswick, NJ).

Table I. Data collection, phasing, and refinement statistics for BTLA

Data Collection <sup>a</sup>		
Space group	P2 <sub>1</sub> 2 <sub>1</sub> 2 <sub>1</sub>	
Unit cell dimensions (Å)	$a = 36.67, b = 37.54, c = 90.15$	
Wavelength (Å)	1.549784	2.066372
x-Ray source	ALS 4.2.2 <sup>b</sup>	ALS 4.2.2
Resolution (Å) (outer shell)	40.0-1.83 (1.92-1.83)	40-2.25 (2.33-2.25)
Observations/unique	66,974/11,536	46,008/6,290
Completeness (%)	95.5 (75.2)	98.9 (92.7)
R <sub>sym</sub> (%)	5.6 (25.7)	9.2 (34.5)
I/σ average	11.7 (4.2)	14.2 (4.0)
Phasing statistics <sup>c</sup>		
Cd <sup>2+</sup> ion sites	2	
R <sub>culis</sub> acentric	0.64	
Phasing power acentric	1.850	
Figure of merit acentric/centric	0.46/0.19	
Refinement summary <sup>d</sup>		
Resolution (Å)	40.0-1.83 (1.92-1.83)	
Reflections R <sub>work</sub> /R <sub>free</sub>	20.6/26.9	
Protein atoms/solvent	846/225	
R <sub>work</sub> overall (outer shell) (%)	35.6	
R <sub>free</sub> overall (outer shell) (%)	44.6	
Rmsd bond length(Å)/angles (°)	0.02/2.20	
Rmsd dihedral/improper (°)	27.7/1.43	
Ramachandran plot		
Most favored/additional (%)	91.4/8.7	
Estimated coordinate error (Å)	0.26 <sup>e</sup>	

<sup>a</sup> Values as defined in d\*TREK (31).

<sup>b</sup> ALS, beamline 4.2.2.

<sup>c</sup> Value as defined in SHARP (33).

<sup>d</sup> Value as defined in CNS (32).

<sup>e</sup> From cross-validated Luzzati plot.

### Surface plasmon resonance (SPR) equilibrium-binding assay

A BIAcore 2000 instrument (GE Health Sciences) was used to determine the affinity of soluble BTLA for murine HVEM-Fc. Between 400 and 1000 resonance units of murine HVEM-Fc, containing CRD1–3, were immobilized to the dextran matrix of a CM5 sensor chip through amine coupling in 10 mM sodium phosphate buffer at pH 5.2 and 5 μl/min. The flow cell had previously been activated with a 1:1 mixture of 0.1 M *N*-hydroxysuccinimide and 0.1 M 3-(*N,N*-dimethylamino)-propyl-*N*-ethylcarbodiimide at a flow rate of 5 μl/min. A related murine TNFR family receptor, RANK, was coupled to an adjacent flow cell as a control for nonspecific binding. The coupling reaction was stopped by injection of 1 M ethanolamine at pH 8.5 for 5 min. Monovalent BTLA was injected over the chip at a flow rate of 20 μl/min. Binding analysis was performed at 25°C in a running buffer of 20 mM sodium HEPES (pH 7.4), 150 mM sodium chloride, and 0.01% Tween 20. All data were analyzed at equilibrium and fit to a simple bimolecular reaction model. The same buffer without added BTLA was flowed past the sensor surface to allow complete dissociation between injections. The production of the murine HVEM ectodomain and the Fc region of human IgG1 as a fusion protein has been described in detail (40).

## Results

### Structure determination of murine BTLA

The N-terminal domain of murine BTLA (BALB/cJ) was expressed in *E. coli* for oxidative refolding by rapid dilution (see *Materials and Methods*). Crystals were obtained in hanging drops of buffered polyethylene glycol 4000. The x-ray diffraction data were collected at the Advance Light Source Synchrotron Radiation Facility (Molecular Biology Consortium Collaborative Access Team, beamline 4.2.2), and extend to a resolution of 1.80 Å. During the crystallization trials, we observed that cadmium ions were required for crystal growth. Indeed, analysis of the anomalous differences in the diffraction data indicated that at least two cadmium ions were associated with each BTLA monomer in the crystal. These ions were sufficient to phase the data by single-wavelength anomalous dispersion methods (41). Data collection and refinement statistics are given in Table I. No density was observed in the model for the first 10 residues of the mature protein, suggesting the

region is disordered. Neither was density observed for the last seven residues, likely to form part of a connecting stalk tethering the protein to the cell membrane.

In the BTLA structure, 10 β-strands are arranged in two sheets to form a compact β sandwich of dimensions 44 × 36 × 31 Å (Ref. 3 and Fig. 1A). The individual sheets consist of the ABED and A'G<sup>0</sup>GFCC' β-strands, respectively (Fig. 1B). This folding arrangement places BTLA within the Ig I-set family (12). Like all I-set domains, the A strand of BTLA starts out antiparallel with B and crosses between the two sheets to finish in parallel with the G strand. The C' strand is not the equivalent of the C' strand found in V and V-like Ig domains but instead cuts across the edge of the β sandwich in what has come to be called a CD transversal strand (12, 42). BTLA contains a disulfide bond linking the B and F strands (connecting the ABED and A'G<sup>0</sup>GFCC' β-sheets), which is a feature common in Ig domains. A second disulfide, unique to BTLA, functions to pin the beginning of the A strand to the end of the B strand. The sequence alignment also suggests that most alleles of BTLA contain a third disulfide, linking the strands at the base of the C-C' loop (Fig. 1C). In this murine BTLA structure (BALB/cJ strain), one half of the disulfide has been replaced by a tryptophan (residue W56 for C56). The hydrophobic tryptophan side chain is completely buried packing against the cysteine residue at position 49. Although a C-C' disulfide linkage is uncommon among Ig domains, similar linkages have been observed in the surface receptors of the NKp44 family (43).

### Characterization of BTLA binding to HVEM by SPR

We set out to determine the binding affinity and kinetic rate constants for the interaction between murine BTLA (BALB/cJ and C57BL/6 strains) and HVEM by SPR analysis. Soluble recombinant BTLA proteins were injected over HVEM-Fc (CRDs 1 through 3) immobilized on a BIAcore sensor chip (Fig. 2A). The

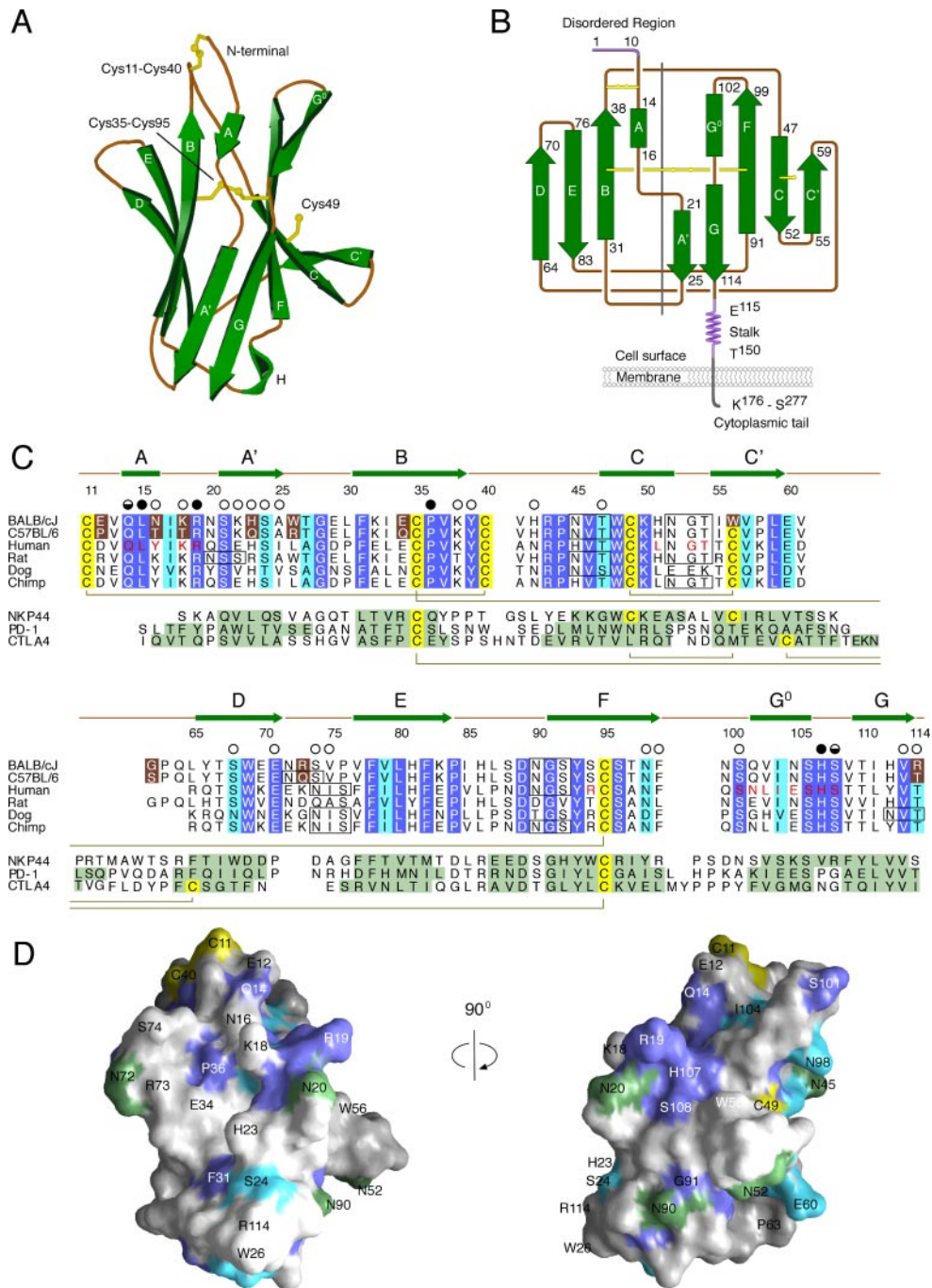


**FIGURE 1.** Three-dimensional structure of the murine BTLA ectodomain. *A*, Ribbon diagram. The membrane proximal surface is oriented toward the bottom. The two sheets are composed of ABED and A'G<sup>0</sup>GFCC'  $\beta$ -strands (green). The disulfides are labeled by their cysteine positions (yellow). *B*, Connectivity diagram of the BTLA fold. A gray line separates the two sheets of the  $\beta$  sandwich. *C*, Structure-based alignment of BTLA with orthologs and the N-terminal domains of related receptors. The secondary structure of BTLA is given at the top with the  $\beta$ -strands colored green and the loops colored brown. Two mouse BTLA sequences (BALB/cJ and C57BL/6) and one human, rat, dog, and chimpanzee are shown (GI:55670802, GI:26334385, GI:31880027, GI:55620804, GI:57109626, and GI:62203073). Allelic polymorphisms between the BALB/cJ and C57BL/6 sequences are boxed in brown. Strictly conserved sequence positions are highlighted in dark blue. Less well-conserved positions (Consurf (51) score > 0.8) are highlighted in light blue. The cysteine positions are boxed in yellow with their disulfide connectivity shown underneath. Potential positions of *N*-linked glycosylation identified by NetNGlyc have been boxed in black. The HVEM-binding study results for the murine BTLA substitutions are summarized above the sequence alignment; filled circles indicate the variant abolished binding, half-filled indicates lowered binding by more than half, open circles indicate it had no effect. Residues that contact HVEM in the human HVEM-BTLA structure are red on the human sequence. A set of related domains is given in an alignment based on their optimal structural superpositions with the BTLA structure (NKp44, a human NK cell receptor PDB ID 1HKF; PD-1, murine programmed death receptor 1 PDB ID 1NPU; murine CTLA-4 PDB ID 1DQT). *D*, BTLA sequence conservation mapped to the molecular surface. The color scheme is the same as in *C* except the potential *N*-linked sites are shown in green. Strictly conserved in dark blue, less well conserved in light blue, the cysteine positions in yellow. The orientation of the surface shown on the left is the same as in *A*.

BALB/cJ and C57BL/6 BTLA proteins differ by 11 of 108 ectodomain residues. The majority of these polymorphisms (6 of 11) occur on the same face of the molecule falling within the A-A'

B strands (Fig. 1C). When the respective equilibrium dissociation constants were measured at steady state, BALB/cJ BTLA yielded a value of  $K_D = 0.97 \pm 0.19 \mu\text{M}$  ( $n = 4$ ) whereas the C57BL/6

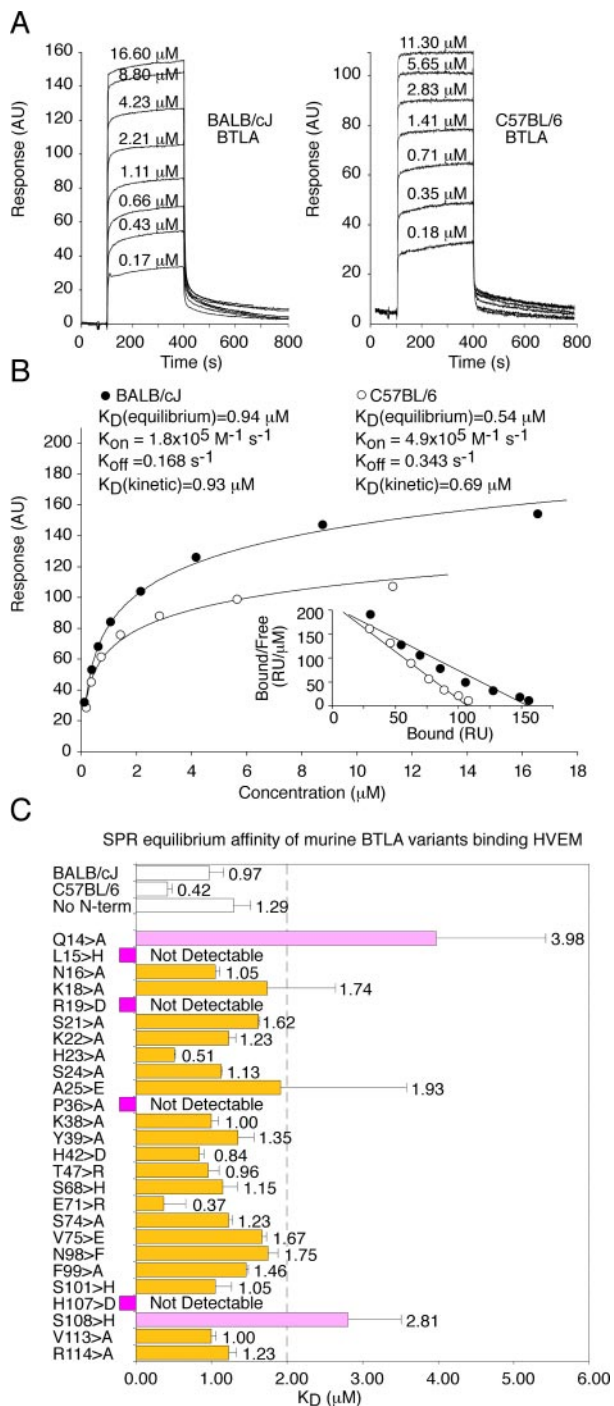


**FIGURE 2.** Steady-state binding of monomeric BTLA to HVEM-Fc. The binding was studied by means of SPR analysis. Native BTLA protein was injected over immobilized HVEM-Fc at the specified concentrations. Approximately 1000 resonance units of the HVEM-Fc were immobilized on the sensor chip. The specific binding was measured as the difference between the response in a sensor chip module coated with HVEM and the response in a module coated with RANK, a related TNFR protein. *A*, Representative binding curves for BALB/cJ and C57BL/6 at the specified concentrations. *B*, Saturation curve of the BALB/cJ- and C57BL/6-specific binding observed at equilibrium under different BTLA concentrations from *A*. Only a small level of nonspecific binding was detected at the protein concentrations used in this study. A Scatchard plot of the binding is shown as an *inset*. In this trial, a  $K_D$  value of  $0.94 \mu\text{M}$  was obtained from the slope of the plot. *C*, Summary of equilibrium-binding data for the various BTLA proteins tested. The variant proteins were named using single-letter amino acid abbreviations to indicate the introduced mutation. For example, the protein where glutamine at position 14 was changed to alanine is named

BTLA bound slightly better, yielding a value of  $K_D = 0.42 \pm 0.06 \mu\text{M}$  ( $n = 3$ ; Fig. 2*B*). Both values are slightly higher than that reported for the binding of soluble gD to human HVEM ( $K_D = 3.2 \mu\text{M}$ ) (44). Although the BALB/cJ BTLA protein binds with slightly lower equilibrium affinity, this is primarily attributable to a decreased on-rate because the half-life of the BALB/cJ BTLA complex is  $\sim 4$  s compared with 2 s for C57BL/6 BTLA. It is important to note that these experiments were done with C57BL/6 HVEM. Although the sequences currently available indicate that polymorphism of murine HVEM is very limited, the sequence of BALB/cJ HVEM has not been reported and therefore it is not known whether the BALB/cJ and C57BL/6 HVEM proteins are identical at the BTLA interaction site.

#### Structure-based mutational analysis of murine BTLA

From these initial studies, we judged that single amino acid substitutions might be sufficient to disrupt these low-affinity interactions. In selecting residues for analysis, we began with a comparison of the available BTLA sequences from different species. Assuming these proteins make similar contacts with HVEM, then the binding surface should be detectable as a patch of conserved residues. Conservation scores for the BTLA sequence alignment (Fig. 1*C*) were calculated and mapped onto the surface of the BTLA structure to identify contiguous patches (Fig. 1*D*). In addition, BTLA is known to be glycosylated *in vivo* and potential binding sites were selected to avoid steric interference by carbohydrate. We were also aided by the software program QUILT which identifies hydrophobic patches on protein surfaces (45), such patches have proven useful in predicting protein-protein interaction sites.

A series of singly substituted BALB/cJ BTLA mutants were constructed and the resulting proteins were analyzed for HVEM binding. Fourteen alanine substitutions (Q14>A, N16>A, K18>A, S21>A, K22>A, H23>A, S24>A, P36>A, K38>A, Y39>A, S74>A, V113>A, F99>A, V113>A, and R114>A), five bulky additions (L15>H, S68>H, N98>F, S101>H, and S108>H), and seven charge substitutions (R19>D, A25>E, H42>D, T47>R, E71>R, V75>E, and H107>D) were tested. The identity of each mutant was confirmed by electrospray mass spectrometry. Each refolded easily, migrated as a monomeric protein on size exclusion chromatography, and ran as a single band on native SDS-PAGE. Two other mutants failed to refold by these criteria and were omitted from the analysis (R73>A and R43>D).

The majority of substitutions tested had little effect (shown in gold, Fig. 2*C*). However, four substitutions (shown in dark magenta, P36>A, L15>H, R19>D, and H107>D) resulted in a greatly diminished affinity of BTLA for HVEM, failing to display detectable binding at concentrations exceeding 10 mM. Two other substitutions (shown in light magenta, Q14>A and S108>H) yielded proteins displaying a greater than 2-fold drop in affinity. These six affected residues cluster close together on BTLA (shown in magenta, Fig. 3, *A* and *B*). These six are invariantly conserved in the sequences of available mammalian species (Fig. 1*C*). Three residues, Q14, L15, and R19, fall within the A strand and the A-A' bulge. Residue R19 is a prominent feature, forming a positively

Q14 > A. BALB/cJ was taken as wild type because the mutants represent single amino acid substitutions of the BALB/cJ protein. No N-term refers to a form of BTLA with the first 10 disordered residues removed. Shown in dark magenta are the substitutions that abolished binding. In light magenta are the substitutions that lowered binding by more than 2-fold. The substitutions with little or no effect are shown in gold. The average  $K_D$  value with SD is given on each bar.

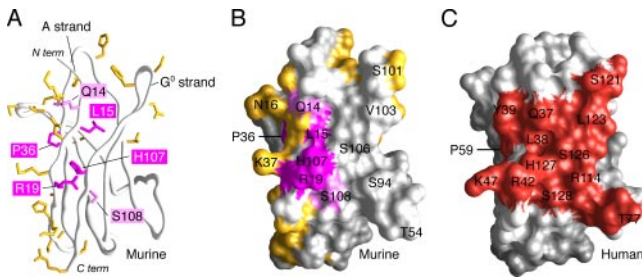


**FIGURE 3.** BTLA residues implicated in HVEM binding by site-directed mutagenesis. *A*, Starting at the left, a tube diagram of BTLA (BALB/cJ) showing the positions of the substituted side chains color coded as in Fig. 2C. Substitutions at the dark magenta positions were found to abolish binding, at the light magenta positions were found to lower binding by more than 2-fold and at the gold positions to have little or no effect. *B*, These values were mapped to the BTLA surface as shown. *C*, For comparison, the human BTLA surface with residues that bury >25% of their solvent-accessible surface upon HVEM binding are red (29). The surface residues are numbered according to their respective structures (mouse BTLA PDB 1XAU, human BTLA PDB 2AW2).

charged projection that juts out from the protein surface. Residue P36 is located close to one side of these three residues on the B strand with its ring also pointing outward. The final two residues H107 and S108 represent part of the G<sup>0</sup>-G bulge and lay at the base of the R19 projection. These results confirm that the HVEM binding site is on the membrane distal face of the BTLA molecule and contains residues from the A strand, the A-A' bulge, and the G<sup>0</sup>-G bulge.

## Discussion

We determined a crystal structure for the extracellular domain of murine BTLA (BALB/cJ) to reveal a  $\beta$  sandwich fold with similarity to I-set members of the Ig superfamily. The BTLA structure bears a resemblance to members of the CD28 family. Like BTLA, the extracellular domains of CD28, CTLA-4, ICOS, and programmed death receptor 1 (PD-1) each consist of a single Ig fold, and each carries a cytoplasmic domain containing tyrosine-dependent signaling motifs. However, significant structural differences exist. First, BTLA is missing the C'' strand found to lie antiparallel to the D strand in all CD28 family members. CD28, CTLA-4, and ICOS assemble into covalently linked homodimers through an unpaired cysteine within their connecting stalks (PD-1 probably also forms a dimer even though it lacks the analogous cysteine residue). BTLA lacks an unpaired cysteine residue in its connecting stalk and our analysis suggests that the presence of *N*-glycosylation at position N90 is likely to prohibit the formation of a CD28-like or CTLA-4-like dimer *in vivo*. The primary binding element used by CD28 family members is contained in the F-G loop. For CTLA-4 and CD28, the ligand-binding surface contains the core hydrophobic residues (MYPPPY), while PD-1 uses ILSPKA (46) and ICOS uses FDPPF (47). The main chain in this region adopts a characteristic *cis-trans-cis*-conformation induced by the *cis*-proline residues. BTLA has a relatively short F-G loop and does not adopt a structurally equivalent conformation. We tested three substitutions within the F-G loop N98>F, F99>A, and S101>H and observed almost no effect on HVEM binding. These results confirm that the BTLA-binding surface is distinct from that used by CD28 family members.

Sequence alignments suggest that most BTLA domains contain an additional disulfide bridge, connecting residues C49 and C56. This disulfide bond is found in members of the NKp44 family where it stabilizes a  $\beta$  hairpin built from the C and C' strands and

the intervening loop. In some NKp44 family members, a surface groove is formed between the two  $\beta$  hairpin loops (C-C' and F-G), which extend out from the face of the molecule. In the case of NKp44, this groove has been shown to bind influenza virus hemagglutinin in the presence of sialic acid (43). In BTLA, the additional disulfide serves to stabilize the C-C' loop which forms one side of the HVEM binding site.

We used the murine BTLA structure to design a mutagenesis study aimed at characterizing the HVEM-binding surface. Solution affinity measurements were obtained between 26 soluble variants of murine BTLA and immobilized HVEM. While this work was in progress, a crystal structure between human BTLA and HVEM was reported (29) (accession no. 2AW2). We have modeled the murine BTLA-HVEM complex based on these results. This could be done with some confidence because the human and mouse HVEM sequences are 62% identical (50 of 80 residues) throughout their CRD1 and CRD2 domains. Still, such analysis can yield only an approximation, although murine HVEM binds human BTLA, human HVEM does not bind murine BTLA (16). Nonetheless, superposition of murine BTLA over the human BTLA coordinates predicts 20 aa within 4.5 Å of HVEM. The majority of these residues can be placed in three groups: seven within the A strand and first part of the following  $\beta$  bulge (E12, Q14, L15, N16, I17, K18, and R19), four at the end of the C-C' loop (H51, G53, T54, and W56), and eight centered on the G<sup>0</sup> strand (S101, Q102, V103, I104, N105, S106, H107, and S108). Five of the six residues implicated by our mutagenesis study (Q14, L15, R19, H107, and S108) fall within this contact region. The sixth residue, P36, falls just outside; even so, it supports the contact region by propping up the A strand.

The proteins encoded by the two most commonly studied murine BTLA alleles (BALB/cJ and C57BL/6) were found to bind murine HVEM with slightly differing affinities (0.94 and 0.42 mM, respectively), with the lower affinity BALB/cJ interactions exhibiting both slower on-rates and off-rates. These differences may be related to the polymorphic tissue distribution of BTLA expression on lymphoid cells in these mice. For example, BTLA in C57BL/6 mice is expressed on T cells, B cells, macrophages, NK cells, and dendritic cells (2). In contrast, BALB/cJ do not express detectable levels of BTLA on macrophage or NK cells. The basis of this expression polymorphism is still unclear. It may represent genetic differences in the regulatory elements controlling BTLA expression or alternately differences in the basal level of lymphoid cell activation. Only 2 of the 11 polymorphic differences between these strains are predicted to fall within the HVEM binding site. Neither could account for the slightly lower affinity of BALB/cJ when examined by alanine substitution (N16>A, K18>A). The small but reproducible difference is probably due to either long-range electrostatic effects or an indirect structural effect on the binding interface. For example, the allelic variation of W56 for C56 may subtly alter the position of the C-C' loop and therefore the HVEM contact interface.

Existing biophysical data indicate that the ectodomains of both BTLA and HVEM are monomeric and that they engage one another with a 1:1 stoichiometry (29). In contrast to previous investigations, we set out to quantitate the monotypic interactions of BTLA with HVEM. For example, Gonzalez et al. (3) used radio-labeled human HVEM-Fc or BTLA-Fc to bind human BTLA- on HVEM-expressing AD-293 cells, obtaining apparent affinities of 5.5 and 15 nM, respectively. Similar studies of bivalent human HVEM-Fc binding to human BTLA expressed on 293T cells gave an apparent affinity of 112 nM, while human HVEM-Fc failed to bind murine BTLA, although murine HVEM-Fc did bind both human (27 nM) and murine (24 nM) BTLA (16). We note that the

low equilibrium affinity of the direct monotypic BTLA-HVEM interaction that we have measured here ( $K_D \sim 1 \mu\text{M}$ ) is more commonly observed for cell surface proteins that are involved in cell surface multimerization or clustering (48), issues that may well be important in BTLA/HVEM signaling.

The response of immune cells, particularly T, B, and NK cells is determined by a constant integration of the activating and inhibitory signals received from their surface receptors. The ability of an Ig-like surface protein to interact with a TNFR superfamily member greatly complicates our understanding of these systems. Until recently, BTLA has been considered strictly an inhibitory regulator of T cell responses, but recent evidence suggests that it may also act in forward signaling to HVEM (49, 50). In the non-irradiated parent-into- $F_1$  graft-versus-host disease (GVHD) model, recent evidence showed a parental cell requirement for HVEM in sustaining reactivity of parental donor cells against the host (49). Surprisingly, BTLA-deficient donor cells showed the same failure to sustain GVHD as shown by HVEM-deficient donor cells (50). BTLA-deficient donor cells underwent initial activation and expansion in vivo following transfer, but failed to survive past 10–11 days, undergoing cell death and exhibiting failure to re-express IL-7R (50). Cotransfer of wild-type donor cells rescued the survival of BTLA-deficient donor cells, indicating a non-cell autonomous action of BTLA in this model. Conceivably, this could be mediated either by a secreted factor produced by wild-type but not BTLA-deficient cells. However, we suggest a mechanism whereby BTLA expression may be required to allow sufficient positive signaling to provide for donor cell survival, a process that may involve additional BTLA interacting partners. Our work in this study identifies variants of BTLA that lack the capacity to interact with HVEM, thus establishing a framework for the investigation of additional BTLA functions in GVHD as well as other experimental models.

## Acknowledgments

We thank Dr. Jay Nix, Beamline Scientist, and the Molecular Biology Consortium Collaborative Access Team at ALS for assistance in crystallographic data collection.

## Disclosures

The authors have no financial conflict of interest.

## References

- Han, P., O. D. Goularte, K. Rufner, B. Wilkinson, and J. Kaye. 2004. An inhibitory Ig superfamily protein expressed by lymphocytes and APCs is also an early marker of thymocyte positive selection. *J. Immunol.* 172: 5931–5939.
- Hurchla, M. A., J. R. Sedy, M. Gavrieli, C. G. Drake, T. L. Murphy, and K. M. Murphy. 2005. B and T lymphocyte attenuator exhibits structural and expression polymorphisms and is highly induced in anergic  $\text{CD4}^+$  T cells. *J. Immunol.* 174: 3377–3385.
- Gonzalez, L. C., K. M. Loyet, J. Calemine-Fenaux, V. Chauhan, B. Wranik, W. Ouyang, and D. L. Eaton. 2005. A coreceptor interaction between the CD28 and TNF receptor family members B and T lymphocyte attenuator and herpesvirus entry mediator. *Proc. Natl. Acad. Sci. USA* 102: 1116–1121.
- Sedy, J. R., M. Gavrieli, K. G. Potter, M. A. Hurchla, R. C. Lindsley, K. Hildner, S. Scheu, K. Pfeffer, C. F. Ware, T. L. Murphy, and K. M. Murphy. 2005. B and T lymphocyte attenuator regulates T cell activation through interaction with herpesvirus entry mediator. *Nat. Immunol.* 6: 90–98.
- Tamada, K., K. Shimozaki, A. I. Chapoval, Y. Zhai, J. Su, S. F. Chen, S. L. Hsieh, S. Nagata, J. Ni, and L. Chen. 2000. LIGHT, a TNF-like molecule, costimulates T cell proliferation and is required for dendritic cell-mediated allogeneic T cell response. *J. Immunol.* 164: 4105–4110.
- Shaikh, R. B., S. Santee, S. W. Granger, K. Butrovich, T. Cheung, M. Kronenberg, H. Cheroute, and C. F. Ware. 2001. Constitutive expression of LIGHT on T cells leads to lymphocyte activation, inflammation, and tissue destruction. *J. Immunol.* 167: 6330–6337.
- Schneider, K., K. G. Potter, and C. F. Ware. 2004. Lymphotoxin and LIGHT signaling pathways and target genes. *Immunol. Rev.* 202: 49–66.
- Watts, T. H. 2005. TNF/TNFR family members in costimulation of T cell responses. *Annu. Rev. Immunol.* 23: 23–68.
- Krieg, C., O. Boyman, Y. X. Fu, and J. Kaye. 2007. B and T lymphocyte attenuator regulates  $\text{CD8}^+$  T cell-intrinsic homeostasis and memory cell generation. *Nat. Immunol.* 8: 162–171.
- Gavrieli, M., J. Sedy, C. A. Nelson, and K. M. Murphy. 2006. BTLA and HVEM cross talk regulates inhibition and costimulation. *Adv. Immunol.* 92: 157–185.
- Watanabe, N., M. Gavrieli, J. R. Sedy, J. Yang, F. Fallarino, S. K. Loftin, M. A. Hurchla, N. Zimmerman, J. Sim, X. Zang, et al. 2003. BTLA is a lymphocyte inhibitory receptor with similarities to CTLA-4 and PD-1. *Nat. Immunol.* 4: 670–679.
- Bernard, D., J. D. Hansen, L. Du Pasquier, M. P. Lefranc, A. Benmansour, and P. Boudinot. 2007. Costimulatory receptors in jawed vertebrates: conserved CD28, odd CTLA4, and multiple BTLAs. *Dev. Comp. Immunol.* 31: 255–271.
- Gavrieli, M., and K. M. Murphy. 2006. Association of Grb-2 and PI3K p85 with phosphotyrosine peptides derived from BTLA. *Biochem. Biophys. Res. Commun.* 345: 1440–1445.
- Gavrieli, M., N. Watanabe, S. K. Loftin, T. L. Murphy, and K. M. Murphy. 2003. Characterization of phosphotyrosine binding motifs in the cytoplasmic domain of B and T lymphocyte attenuator required for association with protein tyrosine phosphatases SHP-1 and SHP-2. *Biochem. Biophys. Res. Commun.* 312: 1236–1243.
- Chemnitz, J. M., A. R. Lanfranco, I. Braunstein, and J. L. Riley. 2006. B and T lymphocyte attenuator-mediated signal transduction provides a potent inhibitory signal to primary human  $\text{CD4}^+$  T cells that can be initiated by multiple phosphotyrosine motifs. *J. Immunol.* 176: 6603–6614.
- Cheung, T. C., I. R. Humphreys, K. G. Potter, P. S. Norris, H. M. Shumway, B. R. Tran, G. Patterson, R. Jean-Jacques, M. Yoon, P. G. Spear, et al. 2005. Evolutionarily divergent herpesviruses modulate T cell activation by targeting the herpesvirus entry mediator cosignaling pathway. *Proc. Natl. Acad. Sci. USA* 102: 13218–13223.
- Krieg, C., P. Han, R. Stone, O. D. Goularte, and J. Kaye. 2005. Functional analysis of B and T lymphocyte attenuator engagement on  $\text{CD4}^+$  and  $\text{CD8}^+$  T cells. *J. Immunol.* 175: 6420–6427.
- Otsuki, N., Y. Kamimura, M. Hashiguchi, and M. Azuma. 2006. Expression and function of the B and T lymphocyte attenuator (BTLA/CD272) on human T cells. *Biochem. Biophys. Res. Commun.* 344: 1121–1127.
- Wang, Y., S. K. Subudhi, R. A. Anders, J. Lo, Y. Sun, S. Blink, J. Wang, X. Liu, K. Mink, D. Degrandi, et al. 2005. The role of herpesvirus entry mediator as a negative regulator of T cell-mediated responses. *J. Clin. Invest.* 115: 711–717.
- Tao, R., L. Wang, R. Han, T. Wang, Q. Ye, T. Honjo, T. L. Murphy, K. M. Murphy, and W. W. Hancock. 2005. Differential effects of B and T lymphocyte attenuator and programmed death-1 on acceptance of partially versus fully MHC-mismatched cardiac allografts. *J. Immunol.* 175: 5774–5782.
- Deppong, C., T. I. Juehne, M. Hurchla, L. D. Friend, D. D. Shah, C. M. Rose, T. L. Bricker, L. P. Shornick, E. C. Crouch, T. L. Murphy, et al. 2006. Cutting edge: B and T lymphocyte attenuator and programmed death receptor-1 inhibitory receptors are required for termination of acute allergic airway inflammation. *J. Immunol.* 176: 3909–3913.
- Montgomery, R. I., M. S. Warner, B. J. Lum, and P. G. Spear. 1996. Herpes simplex virus-1 entry into cells mediated by a novel member of the TNF/NGF receptor family. *Cell* 87: 427–436.
- Kwon, B. S., K. B. Tan, J. Ni, K. O. Oh, Z. H. Lee, K. K. Kim, Y. J. Kim, S. Wang, R. Gentz, G. L. Yu, et al. 1997. A newly identified member of the tumor necrosis factor receptor superfamily with a wide tissue distribution and involvement in lymphocyte activation. *J. Biol. Chem.* 272: 14272–14276.
- Hsu, H., I. Solovyyev, A. Colombero, R. Elliott, M. Kelley, and W. J. Boyle. 1997. ATAR, a novel tumor necrosis factor receptor family member, signals through TRAF2 and TRAF5. *J. Biol. Chem.* 272: 13471–13474.
- Banner, D. W., A. D'Arcy, W. Janes, R. Gentz, H. J. Schoenfeld, C. Broger, H. Loetscher, and W. Lesslauer. 1993. Crystal structure of the soluble human 55 kD TNF receptor-human TNF  $\beta$  complex: implications for TNF receptor activation. *Cell* 73: 431–445.
- Rooney, I. A., K. D. Butrovich, A. A. Glass, S. Borboroglu, C. A. Benedict, J. C. Whitbeck, G. H. Cohen, R. J. Eisenberg, and C. F. Ware. 2000. The lymphotoxin- $\beta$  receptor is necessary and sufficient for LIGHT-mediated apoptosis of tumor cells. *J. Biol. Chem.* 275: 14307–14315.
- Mauri, D. N., R. Ebner, R. I. Montgomery, K. D. Kochel, T. C. Cheung, G. L. Yu, S. Ruben, M. Murphy, R. J. Eisenberg, G. H. Cohen, et al. 1998. LIGHT, a new member of the TNF superfamily, and lymphotoxin  $\alpha$  are ligands for herpesvirus entry mediator. *Immunity* 8: 21–30.
- Jogger, C. R., R. I. Montgomery, and P. G. Spear. 2004. Effects of linker-insertion mutations in herpes simplex virus 1 gD on glycoprotein-induced fusion with cells expressing HVEM or nectin-1. *Virology* 318: 318–326.
- Compaan, D. M., L. C. Gonzalez, I. Tom, K. M. Loyet, D. Eaton, and S. G. Hymowitz. 2005. Attenuating lymphocyte activity: the crystal structure of the BTLA-HVEM complex. *J. Biol. Chem.* 280: 39553–39561.
- Bossen, C., K. Ingold, A. Tardivel, J. L. Bodmer, O. Gaide, S. Hertig, C. Ambrose, J. Tschopp, and P. Schneider. 2006. Interactions of tumor necrosis factor (TNF) and TNF receptor family members in the mouse and human. *J. Biol. Chem.* 281: 13964–13971.
- Pflugrath, J. W. 1999. The finer things in X-ray diffraction data collection. *Acta Crystallogr. D. Biol. Crystallogr.* 55: 1718–1725.
- Brunger, A. T., P. D. Adams, G. M. Clore, W. L. DeLano, P. Gros, R. W. Grosse-Kunstleve, J. S. Jiang, J. Kuszewski, M. Nilges, N. S. Pannu, et al. 1998. Crystallography and NMR system: a new software suite for macromolecular structure determination. *Acta Crystallogr. D. Biol. Crystallogr.* 54: 905–921.

33. Bricogne, G., C. Vornrhein, C. Flensburg, M. Schiltz, and W. Paciorek. 2003. Generation, representation, and flow of phase information in structure determination: recent developments in and around SHARP 2.0. *Acta Crystallogr. D. Biol. Crystallogr.* 59: 2023–2030.
34. Morris, R. J., A. Perrakis, and V. S. Lamzin. 2003. ARP/wARP and automatic interpretation of protein electron density maps. *Methods Enzymol.* 374: 229–244.
35. Jones, T. A., and S. Thirup. 1986. Using known substructures in protein model building and crystallography. *EMBO J.* 5: 819–822.
36. Laskowski, R. A., D. S. Moss, and J. M. Thornton. 1993. Main-chain bond lengths and bond angles in protein structures. *J. Mol. Biol.* 231: 1049–1067.
37. Hubbard, S. J., and J. M. Thornton. 1993. NACCESS Computer Program. Department of Biochemistry and Molecular Biology, University of College London, London, U.K.
38. Nicholls, A., K. A. Sharp, and B. Honig. 1993. The program grasp. *Biophys. J.* 64: 166–170.
39. DeLano, W. L. 2002. *The PyMOL Molecular Graphics System (2002)*. DeLano Scientific, Palo Alto, CA, 2002.
40. Rooney, I., K. Butrovich, and C. F. Ware. 2000. Expression of lymphotoxins and their receptor-Fc fusion proteins by baculovirus. *Methods Enzymol.* 322: 345–363.
41. Dodson, E. 2003. Is it jolly SAD? *Acta Crystallogr. D. Biol. Crystallogr.* 59: 1958–1965.
42. Garapati, V. P., and M. P. Lefranc. 2007. IMGT Colliers de Perles and IgSF domain standardization for T cell costimulatory activatory (CD28, ICOS) and inhibitory (CTLA4, PDCD1 and BTLA) receptors. *Dev. Comp. Immunol.* 31: 1050–1072.
43. Cantoni, C., M. Ponassi, R. Biassoni, R. Conte, A. Spallarossa, A. Moretta, L. Moretta, M. Bolognesi, and D. Bordo. 2003. The three-dimensional structure of the human NK cell receptor Nkp44, a triggering partner in natural cytotoxicity. *Structure* 11: 725–734.
44. Milne, R. S., S. L. Hanna, A. H. Rux, S. H. Willis, G. H. Cohen, and R. J. Eisenberg. 2003. Function of herpes simplex virus type 1 gD mutants with different receptor-binding affinities in virus entry and fusion. *J. Virol.* 77: 8962–8972.
45. Lijnzaad, P., H. J. Berendsen, and P. Argos. 1996. A method for detecting hydrophobic patches on protein surfaces. *Proteins* 26: 192–203.
46. Zhang, X., J. C. Schwartz, X. Guo, S. Bhatia, E. Cao, M. Lorenz, M. Cammer, L. Chen, Z. Y. Zhang, M. A. Edidin, et al. 2004. Structural and functional analysis of the costimulatory receptor programmed death-1. *Immunity* 20: 337–347.
47. Greenwald, R. J., G. J. Freeman, and A. H. Sharpe. 2005. The B7 family revisited. *Annu. Rev. Immunol.* 23: 515–548.
48. Van der Merwe, P. A., and S. J. Davis. 2003. Molecular interactions mediating T cell antigen recognition. *Annu. Rev. Immunol.* 21: 659–684.
49. Xu, Y., A. S. Flies, D. B. Flies, G. Xhu, S. Anand, S. J. Flies, H. Xu, R. A. Anders, W. W. Hancock, L. Chen, and K. Tamada. 2007. Selective targeting of the LIGHT-HVEM costimulatory system for the treatment of graft-versus-host disease. *Blood* 109: 4097–4104.
50. Hurchla, M. A., J. R. Sedy, and K. M. Murphy. 2007. Unexpected role of B and T lymphocyte attenuator in sustaining cell survival during chronic allostimulation. *J. Immunol.* 178: 6073–6082.
51. Landau, M., I. Mayrose, Y. Rosenberg, F. Glaser, E. Martz, T. Pupko, and N. Ben-Tal. 2005. ConSurf 2005: the projection of evolutionary conservation scores of residues on protein structures. *Nucleic Acids Res.* 33: W299–W302.